

Non-minimally coupled gravity as a physically viable fit to DESI 2024 BAO

Gen Ye,^{1,*} Matteo Martinelli,^{2,3} Bin Hu,⁴ and Alessandra Silvestri¹

¹*Institute Lorentz, Leiden University, PO Box 9506, Leiden 2300 RA, The Netherlands*

²*INAF - Osservatorio Astronomico di Roma, via Frascati 33, 00040 Monteporzio Catone (Roma), Italy*

³*INFN - Sezione di Roma, Piazzale Aldo Moro,*

2 - c/o Dipartimento di Fisica, Edificio G. Marconi, I-00185 Roma, Italy

⁴*School of Physics and Astronomy, Beijing Normal University, Beijing 100875, China*

The recent measurements of baryon acoustic oscillations (BAO) from the DESI collaboration have presented an indication for dynamical dark energy, when adopting the (w_0, w_a) parametrization of the equation of state. The associated posterior constraints imply a crossing of the phantom divide. The latter, however, has profound theoretical implications because not all models can do so without developing incurable instabilities. Simple quintessence models of dark energy, for instance, would be ruled out if such a crossing is confirmed. We perform a non-parametric reconstruction of the equation of state, and confirm that crossing of the phantom divide is required by the DESI BAO data. We then explore the theory space of Horndeski gravity employing a reconstruction method based on the effective field theory of dark energy, and show that for most of the models it is still difficult to safely cross the divide. We identify non-minimal coupling to gravity as the key modification which sustains a stable phantom crossing in the general Horndeski theory space and fits DESI observations. Guided by these insights, we propose the *Thawing Gravity* model which has the same number of parameters as $w_0 w_a$ CDM and naturally realizes non-minimal coupling when dark energy becomes non-negligible. *Thawing Gravity* improves the fit over Λ CDM for DESI BAO, CMB as well as type Ia Supernovae.

arXiv:2407.15832v1 [astro-ph.CO] 22 Jul 2024

* ye@lorentz.leidenuniv.nl

I. INTRODUCTION AND SUMMARY

The first data release of DESI baryon acoustic oscillations (BAO) [1, 2] points to a dynamical dark energy (DE) when combined with measurements of the cosmic microwave background (CMB) anisotropy and type Ia Supernovae (SNIa), and analyzed within the w_0w_a CDM scenario. The latter corresponds to a Universe described by general relativity (GR), filled with radiation, ordinary matter, cold dark matter (CDM) and a DE component with an equation of state parametrized as a linear function of the scale factor, i.e. $w_{\text{DE}}(a) = w_0 + w_a(1 - a)$ (CPL) [3, 4]. In the joint analysis with CMB and the Pantheon+ [5], Union [6] or DES Y5 [7] SNIa dataset, the Λ CDM model is excluded at 2.5σ , 3.5σ , 3.9σ , respectively.

This indication of a dynamical dark energy [8, 9] has prompted the exploration of theoretical models that could embed it (see e.g. [10–23]), as well as works that question the robustness of the result [24–35]. For instance, in [11, 27, 35] it has been pointed out that the monopole component of the correlation function of luminous red galaxies at redshift 0.71 plays a significant role in driving the DESI preference for w_0w_a CDM over Λ CDM.

In this work, we would like to focus on one important implication of the DESI results, i.e. that the posteriors for w_0 and w_a imply *crossing of the phantom divide* at low redshift. In other words, the best fit cosmology corresponds to a dynamical DE with an equation of state w_{DE} which crosses -1 [1]. The parameterization of $w_{\text{DE}}(z)$ in terms of w_0 and w_a is however quite simple and this result could in principle be driven by this choice. Before proceeding any further, it is therefore important to verify whether the observed phantom crossing is indeed indicated by DESI observations or is rather an artifact of the chosen parameterization. This question has been discussed in some recent works, e.g. [13, 14, 36]. We address this question in Section III A by performing a *non-parametric* reconstruction of $w_{\text{DE}}(a)$ from DESI data alone and from the joint DESI+CMB+SNIa combination. We find that the hints of a phantom crossing at $z < 1$ are still present, consistently with [8]. This prompts us to explore the gravitational landscape to identify the theory space that would allow a stable phantom crossing.

Phantom crossing has in fact profound implications from a theoretical point of view, as the name may suggest. Quintessence models, consisting of a minimally-coupled scalar field with a standard kinetic term and a potential, cannot cross the phantom divide without exciting ghost instabilities [37]. In fact, for these models one has

$$\rho_{\text{DE}} + P_{\text{DE}} = (1 + w_{\text{DE}})\rho_{\text{DE}} = \dot{\phi}^2, \quad (1)$$

which is always positive. The analysis that we carry out in Section III B confirms these considerations, as summarized in Fig. 1, where we plot the marginalized posteriors for (w_0, w_a) resulting from a fit to the joint DESI+CMB+SNIa dataset. The 2σ contours corresponding to the quintessence model have no overlap with the results obtained assuming an agnostic w_0w_a CDM parameterization with DE perturbations stabilized via the post-friedmann-framework (PPF) like in the DESI analysis [1, 2]. While using the PPF framework can be convenient, it is important to remember that a theoretically viable embedding of the corresponding DE model may require something more sophisticated than quintessence; a model which crosses into the phantom regime, $w_{\text{DE}} < -1$, shall correspond either to a multi-field scenario, e.g. the quintom model [38], more sophisticated DE or modifications of gravity (MG). While in the former case it is possible that DE perturbations remain negligible, and hence the analysis via the PPF framework is a good approximation, in the latter two one needs to consistently account for the modifications also at the level of the dynamics of perturbations (see e.g. [39]).

We focus on DE/MG models that introduce a single scalar dynamical degree of freedom and belong to the broad class of Horndeski gravity [40], described by the following action

$$S = \int d^4x \sqrt{-g} \sum_{i=2}^5 \mathcal{L}_i \quad \text{with} \quad \begin{aligned} \mathcal{L}_2 &= G_2(\phi, X), & \mathcal{L}_3 &= G_3(\phi, X)[\phi], \\ \mathcal{L}_4 &= M_{\text{pl}}^2 G_4(\phi, X)R + G_{4,X}(\phi, X)([\phi]^2 - [\phi^2]), \\ \mathcal{L}_5 &= M_{\text{pl}}^2 G_5(\phi, X)G_{\mu\nu}\phi^{\mu\nu} - \frac{1}{6}G_{5,X}(\phi, X)([\phi]^3 - 3[\phi][\phi^2] + 2[\phi^3]), \end{aligned} \quad (2)$$

where $X \equiv -\frac{1}{2}(\partial\phi)^2$, $\phi_{,\nu} \equiv \nabla_{\mu}\phi$ and square brackets indicate trace of (multiple product of) ϕ^{μ}_{ν} , e.g. $[\phi^2] = \phi^{\mu}_{\nu}\phi^{\nu}_{\mu}$.

We use EFTCAMB [41, 42], a patch to the public Einstein-Boltzmann solver CAMB [43] that implements the effective field theory (EFT) of DE approach [44, 45], to scan efficiently the theory space. A feature of EFTCAMB which is of particular relevance for this work, is its stability module which uses a set of theoretical criteria [41, 42, 46] to check for the viability of a given model. In their basic formulation, these criteria include the conditions for the avoidance of ghost and gradient instabilities, but can also be extended to include no-tachyons conditions [46, 47]. As shown in several works, see e.g. [39, 48, 49], stability conditions can have a significant impact on the final results of cosmological analysis, potentially contributing to a severe limitation of the parameter space. This is relevant not only for the background parameters, in our case (w_0, w_a) , but also for functions parametrizing the dynamics of perturbation [50–52]. In addition to the conditions applied here, further requirements can be imposed on the theory,

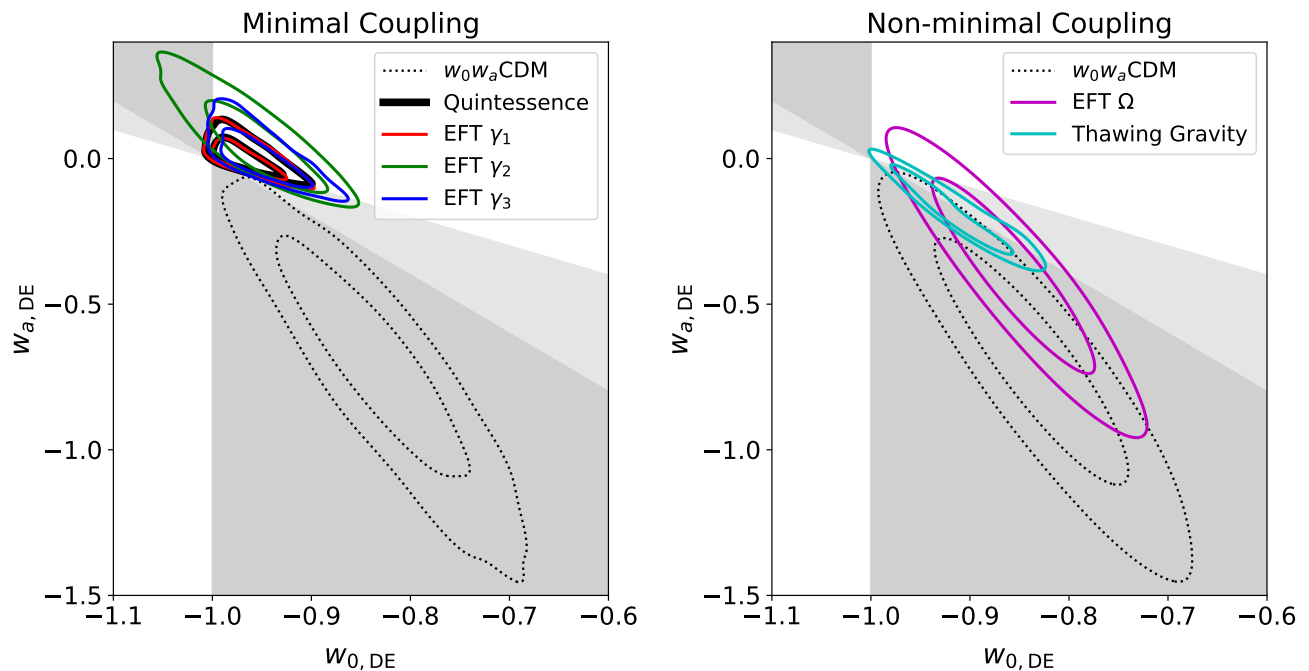


FIG. 1. 68% and 95% marginalized posterior distributions of $w_0 - w_a$ over the joint dataset CMB+DESI+SNIa of all models studied in this paper. The reference $w_0 w_a$ CDM model with PPF DE perturbation is plotted with black dotted contours. The quintessence (black) contour overlaps with the EFT γ_1 result (red) so is plotted with thicker lines. The EFT reconstructions adopt the $\{\Omega, \Lambda, \gamma_1, \gamma_2, \gamma_3\}$ parameterization with $w_0 w_a$ CDM background and are discussed in Section III. *Thawing Gravity* is a non-minimal coupled covariant Horndeski theory described by Eq.(5) in Section IV. Light gray shades mark the parameter regions for which phantom crossing happens, i.e. $(1 + w_0)(1 + w_0 + w_a) < 0$. Dark gray indicates regions where phantom crossing happens at low redshift, $z < 1$, i.e. $(1 + w_0)(1 + w_0 + w_a/2) < 0$.

as those coming from positivity bounds [53, 54]. However, these still suffer from significant uncertainty due to the absence of a robust formulation of the bounds in the cosmological context. Therefore, we do not include them in this analysis. Rather, the condition that will be of central importance for this paper is the no-ghost one, which is intimately related to the phantom crossing.

We use the latest developer version of EFTCAMB, which can work both with the EFT of DE formalism *as well as* directly with any covariant case included in action (2). In the former case, the background and linear dynamics of Horndeski theories are describe via a quadratic action written in the unitary gauge (where constant time hypersurfaces correspond to uniform field ones), as an expansion in operators that are invariant under time-dependent spatial diffeomorphisms up to the quadratic order in perturbations, and lead to second order equations of motion. The operators are generally multiplied by a free function of time, which is dubbed EFT function. We adopt the notation of [55] and write the EFT action as follows

$$\mathcal{S} = \int d^4x \sqrt{-g} \left\{ \frac{M_p^2}{2} (1 + \Omega(\tau)) R + \Lambda(\tau) - c(\tau) a^2 \delta g^{00} + \frac{M_p^2 H_0^2 \gamma_1(\tau)}{2} (a^2 \delta g^{00})^2 - \frac{M_p^2 H_0 \gamma_2(\tau)}{2} a^2 \delta g^{00} \delta K_\mu^\mu - \frac{M_p^2 \gamma_3(\tau)}{2} \left[(\delta K_\mu^\mu)^2 - \delta K_\nu^\mu \delta K_\mu^\nu - \frac{a^2}{2} \delta g^{00} \delta \mathcal{R} \right] \right\} + S_m[g_{\mu\nu}, \chi_m]. \quad (3)$$

It is important to remember that $\gamma_{1,2,3}$ influence only the perturbations while $\{\Omega, \Lambda, c\}$ affect both background and perturbations. In the new covariant option, one needs simply to specify the functional form of the $G_i(\phi, X)$'s and the code solves the full dynamics of both the background and perturbations. This is a very convenient feature which will be soon released with a new public version of EFTCAMB.

We perform a first exploration of the theory space in Section III B, where we open the different EFT functions one at a time and fit the corresponding models to the data, under the no-ghost and no-gradient stability conditions. For this part, we work in the so-called *designer* approach, where we set the background expansion to that of $w_0 w_a$ CDM for all models. In this case, the Friedmann equations can be used to fix both Λ and c , and one is left only with $\{\Omega, \gamma_a, \gamma_2, \gamma_3\}$ as free functions which affect solely the dynamics of perturbations. Crucially, the departures of any of these functions

from their vanishing Λ CDM limit could stabilize the perturbations on a given w_0w_a CDM background that would instead be *unstable* in the quintessence scenario. This is the feature we are after, namely which EFT function would allow a stable crossing of the phantom divide. We do not make any specific choice for the time-dependence of the EFT functions, but rather adopt a non-parametric approach, where we bin them in the scale factor and reconstruct their functional form by fitting them to the data along with (w_0, w_a) and the standard cosmological parameters.

We find that the non-minimal coupling, represented by Ω , is the key to provide a stable phantom crossing scenario. While there may exist specific minimally coupled Horndeski models that allow a stable phantom crossing (e.g. models with kinetic braiding like [56]), they represent some special cases which are hardly picked up with the sampling of the theory space via the EFT formalism. In Fig. 1, we report the posterior contours of (w_0, w_a) for all models explored, dividing them in two classes: minimally and non-minimally coupled. It is evident that only the latter allows the crossing of the phantom divide indicated by the DESI result.

A very recent paper [11] that appeared while we were finalizing our work, has also pointed out that MG effects are generally important to realize the phantom crossing relevant to DESI BAO using the alternative α -based EFT parameterization [57]. However, we stress that it is the clear separation between minimally ($\Omega = 0, \gamma_{1,2,3}$) and non-minimally ($\Omega \neq 0$) coupled scenarios in the $\{\Omega, \gamma_{1,2,3}\}$ parameterization that enables us to single out the non-minimal coupling, amongst all possible MG effects in Horndeski, as the key factor for stabilizing phantom crossing and providing a good fit to the recent DESI BAO observations.

Motivated by the results of this model-agnostic analysis, in Section IV we study a specific covariant, non-minimally coupled Horndeski model, which we dub *Thawing Gravity*. As we will show, this model is able to partially recover the reconstructed phantom crossing from first principles, as can be seen in Fig. 1. With the same number of parameters as w_0w_a CDM, *Thawing Gravity* shows a notably improved fit to all dataset considered, namely CMB, DESI BAO and SNIa, with respect to Λ CDM. It also presents promising potential in unifying both the early and late DE/MG, which will be studied in a future work.

II. DATASETS AND METHODOLOGY

Unless otherwise specified, for all our analyses we use the following joint dataset:

- **DESI:** The full BAO observation from DESI DR1 [1].
- **CMB:** The CamSpec version of Planck PR4 high- ℓ TTTEEE [58] data; Planck 2018 low- ℓ TTEE [59] data; CMB lensing of Planck PR4 [60].
- **SNIa:** Light curve observations of 1550 type Ia Supernovae (SNIa) compiled in the Pantheon+ sample [5].

Cosmological Parameters		Model Parameters	
ω_b	[0.005, 0.1]	w_i	[-6, 1]
ω_c	[0.001, 0.99]	Ω	[-1, 1]
H_0 [km/s/Mpc $^{-1}$]	[20, 100]	γ_1	[-100, 100]
n_s	[0.8, 1.2]	γ_2	[-1, 1]
$\ln 10^{10} A_s$	[1.61, 3.91]	γ_3	[-1, 1]
τ	[0.01, 0.8]	λ	[0.5, 5]
w_0	[-3, 1]	α	[0.1, 1]
w_a	[-3, 2]		

TABLE I. Uniform priors for the cosmological parameters (*left panel*) and the different model parameters (*right panel*)

As already mentioned in Section I, we use the latest developer version (in preparation for release later this year) of EFTCAMB [41, 42] to calculate the cosmology of the different models both at the background and linearly perturbed level. In order to fit the models against the data, we interface this version of EFTCAMB with the public cosmological sampler Cobaya [61, 62] to perform Monte Carlo Markov chain (MCMC) analysis with the Gelman-Rubin diagnostic $R - 1 < 0.02$ [63] as our convergence criteria. All likelihoods used are shipped with the public Cobaya distribution. All the analyses we present in this work have a common set of cosmological parameters, namely: the fractional energy density of CDM and baryons, respectively $\omega_c \equiv \Omega_c h^2$ and $\omega_b \equiv \Omega_b h^2$; the Hubble constant H_0 ; the amplitude A_s and spectral index n_s of the initial curvature perturbation; the effective optical depth τ . For all these parameters we use uninformative flat priors reported in Table I. Priors of model specific parameters are also presented in Table I

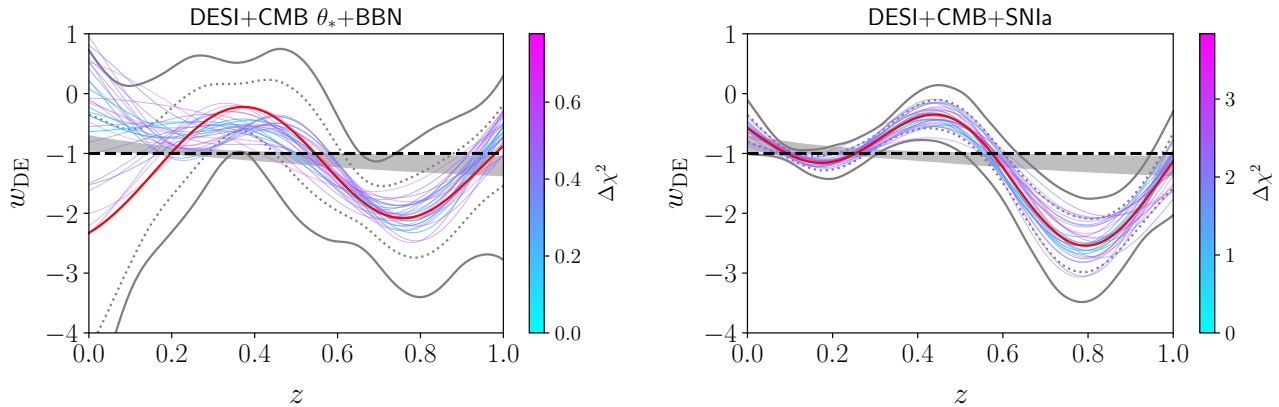


FIG. 2. Reconstructions of $w_{\text{DE}}(a)$ in the redshift range $0 < z < 1$. The black dashed line marks $w_{\text{DE}} = -1$, dotted and solid gray lines indicate the 68% and 95% confidence interval of the reconstructed w_{DE} and the red line plots the mean function. The gray band represents the 95% posterior region of the DESI w_0w_a CDM result. To further illustrate the functional shape preferred by data, we also plot 50 w_{DE} 's from the MCMC sample near the chain bestfit point in terms of χ^2 , with a color coding representing their χ^2 difference $\Delta\chi^2 = \chi^2 - \chi_{\text{bestfit}}^2$. *Left panel:* The minimal reconstruction with DESI BAO alone, aided by a BBN prior and a CMB prior on the angular scale θ_* of recombination sound horizon. *Right panel:* The full reconstruction based on the joint DESI+CMB+SNIa dataset.

but described in their corresponding sections. Following Planck [59], we treat the neutrinos as two massless and one massive with mass $m_\nu = 0.06$ eV reproducing $N_{\text{eff}} = 3.044$ [64–66]. In addition to cosmological and model parameters, we also sample the recommended nuisance parameters for each data likelihood.

III. MODEL-AGNOSTIC APPROACH TO THE DESI BAO OBSERVATIONS

In this Section we focus on non-parametric approaches to the equation of state and to Horndeski gravity in the EFT of DE landscape. As a first step, we reconstruct $w_{\text{DE}}(a)$ directly from the data to establish the evidence for phantom crossing in a parametrization-independent way. We then proceed with surveying the theory landscape in search for models that could sustain a physically stable phantom crossing.

A. Non-parametric reconstruction of the equation of state

We start exploring the robustness of the evidence for phantom crossing against the choice of parametrization for w_{DE} . In fact, the CPL parametrization, defined as

$$w_{\text{DE}}(a) = w_0 + w_a(1 - a). \quad (4)$$

effectively amounts to a linear Taylor expansion around today ($a = 1$) and concerns have been raised regarding its validity at higher redshift and the consequent conclusion of phantom crossing [14, 25, 30, 36]. We do so by performing non-parametric reconstruction of w_{DE} from the observational data. In practice, we model w_{DE} as a general interpolated function of the scale factor over five uniformly spaced nodes at redshifts $z_i = \{0, 0.25, 0.5, 0.75, 1\}$, roughly covering the redshift range of DESI BAO measurements. w_{DE} at $z > 1$ is poorly constrained by data and we assume DE to be subdominant at such high redshift, thus we set $w_{\text{DE}} = -1$ for $z > 1$. We run our MCMC reconstruction pipeline using the node values $w_i = w(z_i)$ as free parameters, assuming the same uniform prior for all of them in Table I, alongside the standard cosmological ones and those controlling the nuisance effects of the used data likelihoods. The w_i 's are interpolated to obtain $w_{\text{DE}}(z)$ and fed to EFTCAMB to compute cosmology. To further assess the impact of DESI BAO and SNIa respectively, we perform two w_{DE} reconstructions. The minimal reconstruction¹ is background only and based on DESI BAO alone, assisted by a BBN prior $\omega_b = 0.02218 \pm 0.00055$ and a CMB prior on the angular scale

¹ In the minimal reconstruction, the perturbation related parameters $\{A_s, n_s, \tau\}$ are irrelevant and fixed to their Planck bestfit values.

$\theta_* = (1.04109 \pm 0.00030) \times 10^{-2}$ of sound horizon at recombination for better convergence [1]. In the full reconstruction we compute the background and linear perturbation cosmology and include the complete information from CMB and SNIa by using the joint DESI+CMB+SNIa dataset described in Section II. In the latter case DE perturbations are taken into account with PPF.

The reconstructed $w_{\text{DE}}(z)$ from both the minimal and full reconstructions, obtained marginalizing over all parameters except for the w_i 's, are shown in Fig. 2. The CPL parameterization of DESI is plotted as a gray band, and it can be noticed that it captures the mean shape of the reconstructed w_{DE} in the full reconstruction case. While both panels in Fig. 2 display a clear preference ($\geq 2\sigma$) for $w < -1$ at $z > 0.6$, it is the SNIa data that constrains $w_{\text{DE}} > -1$ at $z = 0$ at 2σ , which consequently leads to the phantom crossing conclusion assuming a continuous w_{DE} . This observation is consistent with the finding of DESI [1] when fitting $w_0 w_a$ CDM to DESI BAO and DESI BAO+SNIa. Let us notice that DESI performed also a reconstruction of w_{DE} , by expanding it in Chebyshev polynomials in [8]. Even though our methods differ, the results are consistent in that both imply a phantom crossing at low redshift². In Fig. 1, we plot also 50 different realizations of $w_{\text{DE}}(z)$ taken from the MCMC sample, selecting those that have a small $\Delta\chi^2 = \chi^2 - \chi_{\text{bestfit}}^2$, where χ_{bestfit}^2 is the chain bestfit. The curves are colored according to the magnitude of the corresponding $\Delta\chi^2$, as indicated by the legend on the right of the plots. They offer an interesting insight into the functional forms for w_{DE} preferred by the joint dataset.

Our main focus here is to establish the evidence for phantom crossing in the observations, rather than focusing on the detailed reconstructed shape of w_{DE} . For this reason, we avoid including any theory driven correlation prior, as well as any specific functional form such as the Chebyshev polynomials used in [8], in our reconstruction to ensure that we rely solely on information from the data. The caveat of this approach is the risk of overfitting the data, and the oscillatory features in Fig. 2 might be in fact due to that. See for instance [68, 69] for a discussion about this. However, the general trend of the reconstructed curve, and more specifically of its 95% confidence interval, shows that $w_{\text{DE}} > -1$ at $z = 0$ and $w < -1$ for $z > 0.6$ at 2σ level, in agreement with the reconstruction from DESI using a different method [8] as well as the $w_0 w_a$ CDM result (gray band), and provides support for a phantom crossing at low redshift.

Given these results, we are further motivated to explore the theory space in search of models that allow a safe *crossing* of the phantom barrier.

B. Exploration of phantom crossing within the EFT of DE

We survey the gravitational landscape using the unifying framework of EFT of DE, which we described in Section I. Since our focus is to identify EFT operators that would allow for a physically viable embedding of the best fit DESI cosmology, we work in the designer approach, i.e. we fix the background to a $w_0 w_a$ CDM one, and work with the remaining four EFT functions $\{\Omega, \gamma_1, \gamma_2, \gamma_3\}$. In the same spirit of Section III A, we avoid using parametrizations, and rather bin the EFT functions in time using six nodes at $a \in [0.5, 0.6, 0.7, 0.8, 0.9, 1.0]$, corresponding to the redshift range $0 < z < 1$ most relevant to data. Starting from these nodes, we use a Gaussian Process interpolator³ to generate a smooth function in $0 < z < 9$. It interpolates between the nodes within the node range $0 < z < 1$ ($1 > a > 0.5$) and smoothly extrapolates to the mean value of the nodes outside of the interpolation range. The interpolator outputs a much finer tabulate of function values which is then fed to EFTCAMB for the calculation of the cosmological dynamics. Since we are focusing on DE, we set EFTCAMB to only switch on the EFT equations at $z = 9$, and the dynamics is evolved with standard general relativity until then, equivalent to setting all EFT functions to zero for $z > 9$.

We use the same prior, reported in Table I, for all nodes of the EFT functions. Only in the case of γ_1 , we use inflated priors, part of which are even beyond perturbative control in linear EFT, because it is known that kineticity is very poorly constrained (see e.g. [70, 71]). We find that the joint DESI+CMB+SNIa dataset does not have enough constraining power when all EFT functions are kept free at the same time⁴ and therefore opt for the more conservative choice of varying one EFT function at a time, fixing the remaining ones to their Λ CDM value. While such approach will not cover the full space of models within the EFT of DE, it has the advantage of allowing us to isolate more clearly the function, and the corresponding EFT operator, that allows for a safe phantom crossing.

After performing a combined fit to the joint dataset, we obtain confidence intervals for w_0, w_a and the other cosmological parameters, as well as *reconstructed* EFT functions, which we show in Appendix A. We present the contours for (w_0, w_a) in Fig. 1, together with those for a simple $w_0 w_a$ CDM cosmology treated via the PPF parametrization and for a quintessence embedding of $w_0 w_a$ CDM, obtained by setting the four EFT functions $\{\Omega, \gamma_1, \gamma_2, \gamma_3\}$ to their vanishing GR limit in the EFT approach.

² Ref.[67] reports somewhat different results from both ours and that of [8], probably due to the different dataset used.

³ We use the square exponential kernel with the correlation length set to equal to the node spacing $\Delta a = 0.1$. The variance is set to be much smaller than the constraining power of data thus there is effectively no randomness in the interpolated function.

⁴ We tried to reconstruct jointly γ_1 and γ_2 , however the analysis could not reach convergence within a reasonable time.

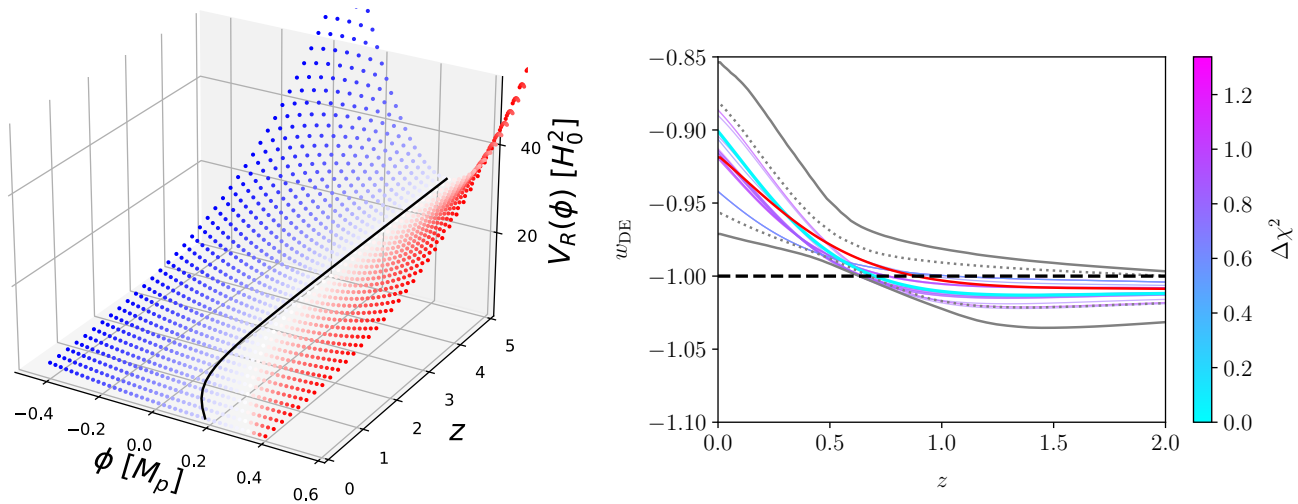


FIG. 3. *Left panel:* Shape of the curvature dependent effective potential $V_R(\phi)$ of the non-minimal coupling theory (5), with $\xi = 0.65$, $\lambda = 1.4$, $V_0/3H_0^2 = 0.72$ taken from the bestfit cosmology. Potential surface is colored with respect to the strength of its gradient in the ϕ direction, with red for positive, blue for negative and white for $dV_R/d\phi = 0$. Black solid line depicts the field trajectory output by the new EFTCAMB. *Right panel:* Constraints on the functional shape of w_{DE} in the *Thawing Gravity* model (5). The gray dotted and solid lines represent the 68% and 95% posterior regions, respectively. Black dashed line marks the position of $w_{DE} = -1$. To further illustrate the w_{DE} shape in the DESI+CMB+SNIa constrained *Thawing Gravity* model, we also plot 50 w_{DE} 's from the MCMC sample near the chain bestfit point in terms of χ^2 , with a color coding representing their χ^2 difference $\Delta\chi^2 = \chi^2 - \chi_{\text{bestfit}}^2$.

The clear message from Fig. 1 is that the EFT functions $\{\gamma_{1,2,3}\}$, when turned on one by one, are unable to reliably stabilize phantom crossing, and in fact all posteriors are limited by the gray region representing phantom crossing. Only Ω is able to lead the sampled EFT into the dark gray phantom crossing region where the DESI result resides.

In summary, from Fig. 1 we conclude that the crossing of the phantom divide is in general very hard to stabilize, with EFT Ω being the only model in Fig. 1 able to push the (w_0, w_a) posterior into the phantom crossing region favored by DESI. All this, implies that non-minimal coupling offers ample ways of stabling crossing the phantom barrier, and, furthermore, it is *the* key EFT ingredient within the broad Horndeski framework that does so.

IV. THAWING GRAVITY APPROACH TO DESI OBSERVATIONS

The non-parametric approaches used in the previous Section are optimal for systematically extracting information from data while swiping a large space of viable theories. They point towards the sector of non-minimally coupled gravity models as candidates to safely cross the phantom divide and fit well the joint DESI+CMB+SNIa dataset. In this section we turn to the covariant formulation in search for a non-minimally coupled model within action (2) that would provide a good fit and a stable phantom crossing from first principles. To this extent, we consider models with a non-trivial $G_4(\phi)$, and identify the following Lagrangian

$$L = \frac{M_p^2}{2} [1 - \xi(\phi/M_p)^2] R + X - V_0 e^{-\lambda\phi/M_p}, \quad (5)$$

where $\{\xi, V_0, \lambda\}$ are constant parameters and we consider the $\xi > 0$ case in this paper.

This is a non-minimally coupled model with a luminal speed of propagation both for gravitational waves and the scalar field, hence it is free from gradient instabilities. As for the sign of the kinetic term, the model is safe from ghost when $\xi > 1/6$, while for $0 < \xi < 1/6$ the no-ghost condition reads $\xi\phi^2 < \frac{1}{1-6\xi}$. However, in the latter case the background solution becomes pathological due to the effective Planck mass $M_{\text{eff}}^2 = (1 - \xi\phi^2)M_p^2$ becoming negative (before the no-ghost condition breaks), which in practice is prohibited by mathematical conditions within EFTCAMB. As a result, the no-ghost and no-gradient stability conditions contribute no new constraints to the theory.

The model has a curvature dependent effective potential

$$V_R(\phi) = \frac{1}{2}\xi R\phi^2 + V_0 e^{-\lambda\phi/M_p}, \quad (6)$$

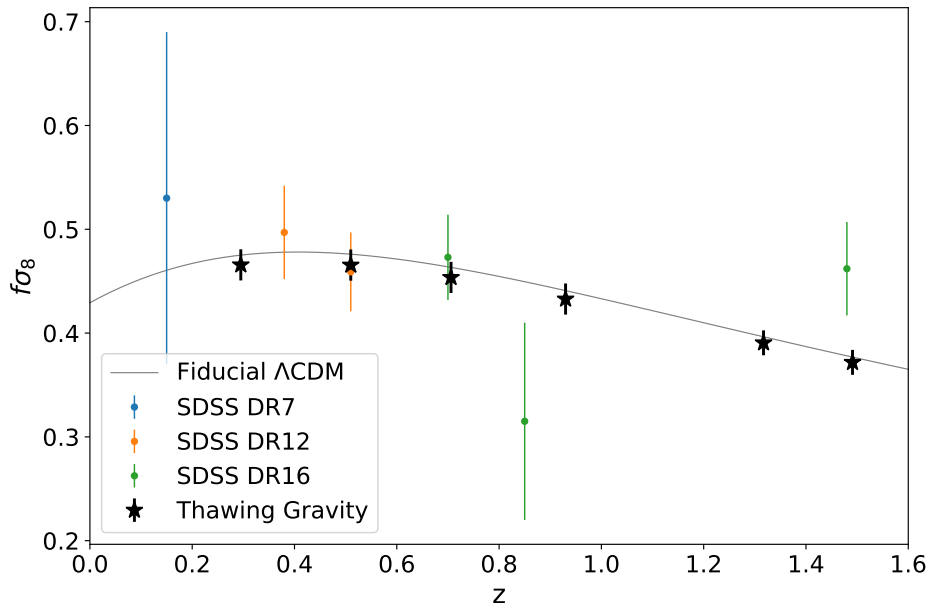


FIG. 4. Mean and 3σ posterior of $f\sigma_8(z)$ of the *Thawing Gravity* model at the effective redshifts $z = 0.295, 0.510, 0.706, 0.930, 1.317, 1.491$ of DESI BAO. For reference we also include previous $f\sigma_8$ measurements from the SDSS DR7 [72], DR12 [73] and DR16 [74] with error bar indicating the 1σ variance. Solid black line is the $f\sigma_8(z)$ from the bestfit Λ CDM of Planck 2018.

with one global minimum for $\xi > 0$. The curvature dependence provides an interesting dynamics, with the field frozen at the minimum of the effective potential at early times, when R is large during matter era, and then gradually starting to evolve under the effect of the self-interacting potential. When R dominates, more specifically when $\xi M_p^2 R \gg \lambda V_0$ and $\xi M_p^2 R \gg \lambda^2 V_0$, the global minimum is close to zero

$$\phi_m \simeq \frac{\lambda V_0}{\xi M_p^2 R + \lambda^2 V_0} M_p \sim 0, \quad \text{with} \quad m_\phi^2|_{\phi=0} = \frac{d^2 V_R}{d\phi^2} = \xi M_p^2 R + \lambda^2 V_0. \quad (7)$$

At early times (still in matter era), as long as ξ is not too small, the R dependent part of m_ϕ^2 is much larger than $\lambda^2 V_0$ (which approximates the DE energy scale), the field evolution is dominated by the quadratic part of Eq. (6) and ϕ is localized at the global minimum ϕ_m . As the Universe expands and R decreases, the second term in m_ϕ^2 starts dominating and the field starts rolling along its potential $V_0 e^{-\lambda\phi/M_p}$, effectively thawing and deviating from ϕ_m . This leads to an effective Planck mass $M_{\text{eff}}^2 \equiv (1 - \xi\phi^2)M_p^2$ which decreases with time. We dub the model *Thawing Gravity*. Fig. 3 further illustrates this dynamical picture. We plot the effective potential $V_R[\phi(z)]$ as a two dimensional surface and the field evolution trajectory, for the bestfit model from our joint DESI+CMB+SNIa analysis. We use a color coding to indicate the magnitude of the gradient of the potential, $dV_R/d\phi$. It can be noticed that the field trajectory starts deviating from the local minimum (which corresponds to the white valley in the potential surface), effectively thawing, at low redshifts.

Fig. 3 displays the full background solution which we derive, along with the dynamics of linear perturbations, using a new *Horndeski module* of EFTCAMB, which will soon be released with a new version of the code. This module allows the user to work directly with any covariant Lagrangian belonging to the Horndeski class. Differently from the original EFT approach, where the additional dynamics is evolved via the equation for the Goldstone field $\pi = \delta\phi/\dot{\phi}$, this new module solves the background and perturbation equations of ϕ and $\delta\phi$ for any arbitrary choice of $G_i(\phi, X)$. It represents a major addition to the original code, which has the added advantage of handling better the cases where $\dot{\phi}$ changes sign, a feature of oscillating DE/MG models which is numerically challenging in the EFT implementation due to the divergence in the dynamical variable π . We focus on the era relevant to DE and DESI observations, thus we start evolving ϕ and $\delta\phi$ at $a = 0.01$ with the initial condition $\phi_{\text{ini}} = \dot{\phi}_{\text{ini}} = \delta\phi_{\text{ini}} = 0$. For all $a < 0.01$ we set $\delta\phi$ and its derivatives to zero, effectively evolving GR equations.

We perform a fit to CMB+DESI+SNIa to determine the posterior constraints and bestfit values of the model and cosmological parameters. Among the three parameters $\{\xi, V_0, \lambda\}$ of Eq.(5), only $\{\xi, \lambda\}$ are free while V_0 needs to be adjusted, at every MCMC step, by a shooting algorithm to ensure that the resulting $H_0 = H(z=0)$ matches the H_0

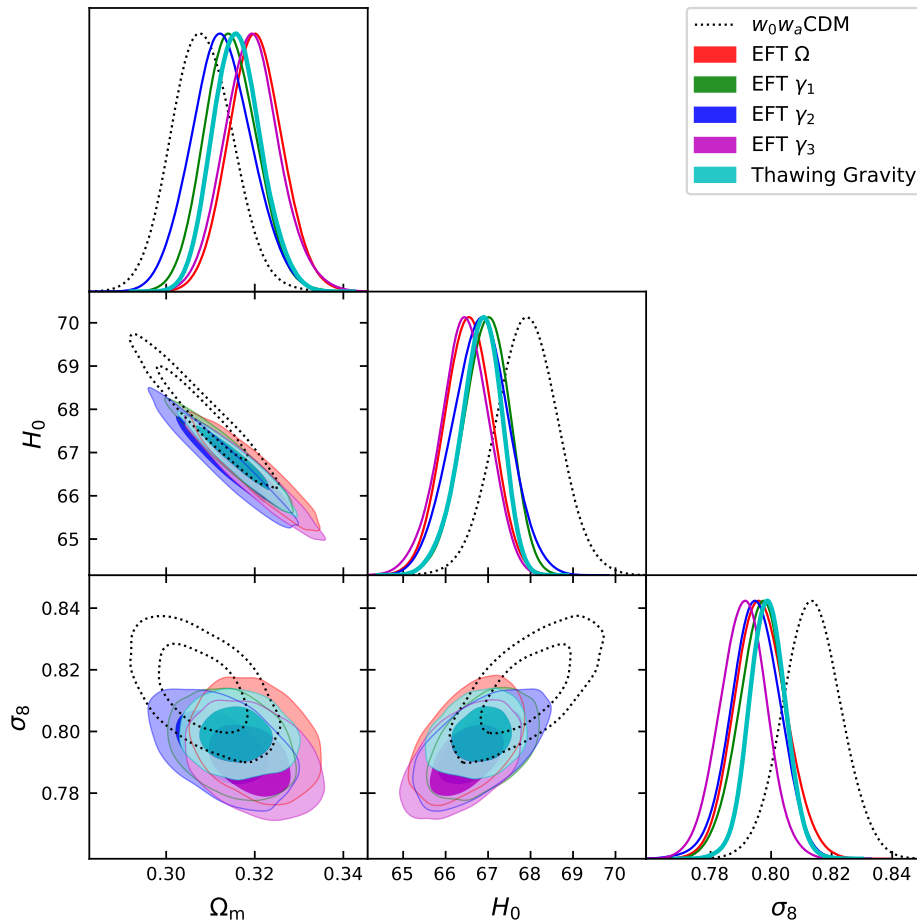


FIG. 5. 68% and 95% marginalized $\Omega_m - \sigma_8 - H_0$ posterior distributions of the EFT and *Thawing Gravity* models.

input parameter of the MCMC, with a tolerance of 0.1%. In the MCMC analysis, we replace ξ with

$$\alpha \equiv \frac{3M_p^2 H_0^2}{\lambda^2 V_0} \xi \quad (8)$$

as the sampled parameter, since it represents a convenient, dimensionless parameter that approximately parameterizes the time of thawing according to Eq. (7).

Overall *Thawing Gravity* has the same number of parameters as $w_0 w_a$ CDM, i.e. $\{\omega_c, \omega_b, H_0, \ln 10^{10} A_s, n_s, \tau, \lambda, \alpha\}$. We show our choices for the priors in Table I. The model reduces to standard quintessence DE at both $\xi \rightarrow 0$ and $\xi \rightarrow +\infty$, corresponding to $\alpha \rightarrow 0$ and $\alpha \rightarrow +\infty$ with finite λ . For the purpose of this study we restrict to the parameter space corresponding to phantom crossing and thus adopt a prior on α that excludes both cases.

We collect the detailed MCMC products in Appendix B. Here, in the right panel of Fig. 3, we show the results of $w_{\text{DE}}(z)$ calculated as

$$w_{\text{DE}} \equiv \frac{-2\dot{H} - 3H^2 - P_m}{3H^2 - \rho_m} \quad (9)$$

where subscript “m” refers to the total energy density or pressure of all species except for the DE field. Like in Fig. 2, in addition to the 1σ and 2σ posteriors, we also plot out 50 w_{DE} trends clustering around the chain bestfit point, representing the models that are most preferred by the data. All of the plotted w_{DE} trends, as well as the mean function, display phantom crossing behavior in $0.5 < z < 1$, consistent with what we observe in the non-parametric reconstruction of w_{DE} in Section III A.

Fig. 3 indicates that for the *Thawing Gravity* model the linear approximation of CPL works to some extent in the redshift range $0 < z < 1$. We thus derive the effective w_0, w_a parameters for each point in the MCMC chain by least

square fitting the actual $w_{\text{DE}}(a)$ to the CPL form Eq.(4) in $0 < z < 1$. The resulting (w_0, w_a) posterior is shown in Fig. 1; one can notice that it appears skewed, as expected, since it is associated to a linear approximation of the actual, theoretically derived w_{DE} . As can be noticed also in Figs. 1 and 3, *Thawing Gravity* provides a theoretical, covariant realization of the reconstructed EFT Ω as well as a natural way to implement phantom crossing in favor of DESI BAO. *Thawing Gravity* also fits better all data in the joint the dataset, with $\Delta\chi_{\text{DESI}}^2 = -2.1$, $\Delta\chi_{\text{CMB}}^2 = -1.8$ and $\Delta\chi_{\text{SNIa}}^2 = -1.9$ compared with ΛCDM .

Being a non-minimally coupled MG theory, *Thawing Gravity* modifies the growth of perturbations. While in this paper we do not focus on the large scale structure, it is still interesting to have a look at the prediction for clustering. To this extent, we extract the growth rate $f\sigma_8(z) \equiv \frac{d\log\sigma_8(z)}{d\log a}$, where $\sigma_8(z)$ is the average amplitude of matter perturbation in a sphere of diameter $8h^{-1}$ Mpc at redshift z . We plot the mean and posterior of $f\sigma_8(z)$ for *Thawing Gravity* in Fig. 4. Since we find that $f\sigma_8$ is highly constrained, with a very small 1σ range (thanks to the inclusion of full CMB in the dataset), we plot in Fig. 4 the 3σ posterior. For reference we also plot the $f\sigma_8(z)$ measurements by the SDSS DR7 [72], DR12 [73] and DR16 [74]. The growth in *Thawing Gravity* deviates slightly from the reference ΛCDM at low redshift when gravity thaws, but still not significantly enough to be picked up with current $f\sigma_8$ measurements as shown in Fig. 4. Fig. 5 further shows the 2D posterior distributions of $\Omega_m - \sigma_8 - H_0$ (where $\sigma_8 = \sigma_8(z=0)$), in comparison with those obtained from the EFT reconstructions and the reference $w_0w_a\text{CDM}$ model. All MG models predict smaller σ_8 than $w_0w_a\text{CDM}$, as preferred by the weak lensing measurements [75–78].

V. FINAL REMARKS

The recent DESI DR1 BAO results, if confirmed, point to dynamical DE rather than a cosmological constant, with a $w_0w_a\text{CDM}$ cosmology preferred at $\sim 3\sigma$ over ΛCDM . Further, the confidence intervals for (w_0, w_a) indicate a DE which crossed the phantom barrier at low redshift. In this paper, we have investigated the theoretical implications of this finding. To start with, we have analyzed the DESI data with a non-parametric approach in order to establish the evidence for phantom crossing independently from the use of any specific parametrization, in this case the CPL one. We have binned w_{DE} in time and reconstructed its functional form without prior theoretical knowledge, finding indication for phantom crossing at $z < 1$ in both the DESI and DESI+CMB+SNIa data, see Fig. 2, in agreement with [9].

Motivated by this result, we have set out on a survey of the gravitational landscape, to identify models that could provide a theoretically viable embedding of the DESI result. It is well known in fact, that quintessence cannot cross the phantom barrier without exciting the ghost instability [37]. We used the unifying framework of EFT of DE, which encompasses scalar-tensor theories with second order equations of motion, to explore all models belonging to the broad class of Horndeski gravity. Using the latest developer version of EFTCAMB, soon to be released, we have identified non-minimal coupling as the key ingredient to realize the phantom crossing preferred by DESI within the general Horndeski theory space. Fig. 1 summarizes this result, showing very clearly that minimally coupled models, as well as quintessence, cannot break into the phantom-crossing region indicated by DESI, with their 2σ contours flattened against the stability bounds. In both panels of Fig. 1, we show also the contour corresponding to $w_0w_a\text{CDM}$, which, like for the DESI analysis, relies on the PPF parametrization to artificially stabilize the DE perturbations. The quintessence model, on the other hand, has also a $w_0w_a\text{CDM}$ background, but is subjected to the no-ghost and no-gradient conditions that come with its embedding into a single field theory. From the right panel of Fig.1, it is evident that non-minimally coupled DE, characterized by the EFT function $\Omega(z)$, offers ample opportunities to cross the phantom divide in a theoretically viable way. In this case, the 2σ contours for (w_0, w_a) show significant overlap with those of $w_0w_a\text{CDM}$, entering all the way into the dark grey region that corresponds to crossing at $z < 1$. It is very powerful to see how the EFTofDE, in its $\{\Omega, \gamma_1, \gamma_2, \gamma_3\}$ formulation has allowed us to single out *the* MG feature which is implied by the DESI BAO results.

The model-agnostic analysis pointed us towards the space of non-minimally coupled gravity models as candidates to safely cross the phantom divide while fitting the joint DESI+CMB+SNIa data. Motivated by this significant finding, we turned to the covariant action for scalar-tensor theories, and in particular its non-minimal coupling part, to find first principles realizations. We identified a candidate model, which we dubbed *Thawing Gravity* since the scalar field is initially frozen and thaws at low redshift, leading to a dynamics that fits well the DESI+CMB+SNIa data, with $\Delta\chi_{\text{DESI}}^2 = -2.1$, $\Delta\chi_{\text{CMB}}^2 = -1.8$ and $\Delta\chi_{\text{SNIa}}^2 = -1.9$ compared to the ΛCDM case. *Thawing Gravity* still has a slightly bigger χ^2 than $w_0w_a\text{CDM}+\text{PPF}$ with $\Delta\chi_{\text{tot}}^2 = 1.6$, see Appendix B. However, it has the important advantage, over $w_0w_a\text{CDM}+\text{PPF}$, of being a fully covariant model that describes both background and perturbation dynamics consistently. We were mostly interested in the dynamics at low redshift, therefore we focused on the evolution of the scalar field at times well after recombination. As a side note, we shall note that the same model could be a natural candidate for early dark energy (EDE) and early modified gravity (EMG) [79–85] since even with general non-zero initial conditions at an initial time before recombination, the field might still be dynamically stabilized to $\phi \simeq 0$ near

matter-radiation equality when the curvature R becomes non-zero [79–85]. We leave the exploration of the possibility of unifying EDE/EMG with DE/MG with this model for future work. Also, since BAO observations are an important consistency test of CMB in terms of the sound horizon scale which also breaks certain degeneracy in CMB, it will be also interesting to consider the impact of DESI BAO on general pre-recombination models, see [86–92] for some recent studies.

While our focus was on the DESI BAO results, we have looked also at the prediction of *Thawing Gravity* for the growth rate of structure, $f\sigma_8(z)$, see Fig. 4 and 5. Further study is required to investigate its impact on the galaxy survey and weak lensing observables and to correctly account for its effect on the non-linear evolution.

In conclusion, as we have highlighted in this paper, any indication of a preference for phantom crossing is bounded to bring with itself relevant theoretical implications. To this extent, it is natural that the recent results from DESI BAO have prompted numerous investigations on the theory side. However, it is worth stressing that the evidence still needs to be corroborated, as it is often the case with hints at $2 - 3\sigma$ level in new data.

ACKNOWLEDGMENTS

GY thanks Yun-Song Piao for insightful discussions. Some of the plots were made with `GetDist` [93]. The authors acknowledge computational support from the ALICE and Xmaris clusters of Leiden University. The cosmology code used is a major component of the new `EFTCAMB` (in preparation) which will be made public later this year. GY and AS acknowledge support from the NWO and the Dutch Ministry of Education, Culture and Science (OCW) (through NWO VIDI Grant No. 2019/ENW/00678104 and ENW-XL Grant OCENW.XL21.XL21.025 DUSC) and from the D-ITP consortium. MM acknowledges funding by the Agenzia Spaziale Italiana (ASI) under agreement no. 2018-23-HH.0 and support from INFN/Euclid Sezione di Roma. BH is supported by the National Natural Science Foundation of China Grants No. 12333001.

Appendix A: Details of the EFT reconstruction

Fig. 6 plots the four reconstructed EFT functions using the joint DESI+CMB+SNIa dataset. Solid and dotted gray lines mark the 68% and 95% posterior region of the reconstructed function values at each redshift, while the mean function is plotted as red lines, providing a rough indication of the function shape and scale. Lines with a color coding are 50 reconstructed functions clustered near the chain bestfit with their distance from the bestfit point indicated by $\Delta\chi^2 = \chi^2 - \chi_{\text{bestfit}}^2$. These lines represent the function shapes that are most favored by the joint dataset.

Looking at Fig. 6 one can appreciate that the reconstructed non-minimal coupling $\Omega(z)$, shown in the upper left corner is significantly more constrained than the other EFT functions, with the 2σ contour remaining between 0 and 0.1. Also, the lower 95% confidence contour lies at $\Omega > 0$, indicating a preference at 2σ for a non-minimal coupling. This is in agreement with the corresponding contours for (w_0, w_a) shown in Fig. 1. Despite of the inflated prior, γ_1 is still prior dominated in Fig. 6, confirming that kineticity is hardly constrained by observation, as seen already e.g. in [70, 71]. γ_2 is related to kinetic braiding and is reconstructed to be negative at 2σ in Fig. 6. Also the corresponding EFT γ_2 contour in Fig. 1 extends to the gray region in the upper left quadrant, i.e. a DE which is quintessence-like in the past and phantom-like today (opposite to the indication of DESI). Interestingly, this is consistent with the expectation of the Galileon kinetic braiding model in Ref. [56]. The γ_3 reconstruction in Fig. 6 prefers $\gamma_3 \geq 0$, corresponding to (sub-)luminal tensor speed, consistent with the finding of Ref. [54] for the case without positivity bounds. Note however that Ref. [54] also found the opposite preference, i.e. $\gamma_3 \leq 0$ and (super-)luminal tensor speed, if positivity bounds are included. Except for the prior dominated γ_1 , there is either an increasing or decreasing trend observed in the reconstructed EFT functions $\{\Omega, \gamma_2, \gamma_3\}$ at $z < 0.5$.

Fig. 9 further plots the marginalized posterior distributions of all cosmological parameters in the EFT reconstructions.

Appendix B: Details of the *Thawing Gravity* model

In Fig. 7 we plot the EFT function Ω corresponding to the *Thawing Gravity* model, derived from the full dynamics solution of each point in the MCMC chain. It is worth pointing out that it gives $\Omega_{\text{thawing}} < 0$, of the opposite sign w.r.t. reconstructed one in Fig. 6, but still indicates a clear preference for non-minimal coupling and a decreasing trend of Ω near $z = 0$, the latter of which is also observed in the reconstruction in Fig. 6. The sign difference is not surprising since the reconstruction uses a designer approach, and samples one EFT function at a time.

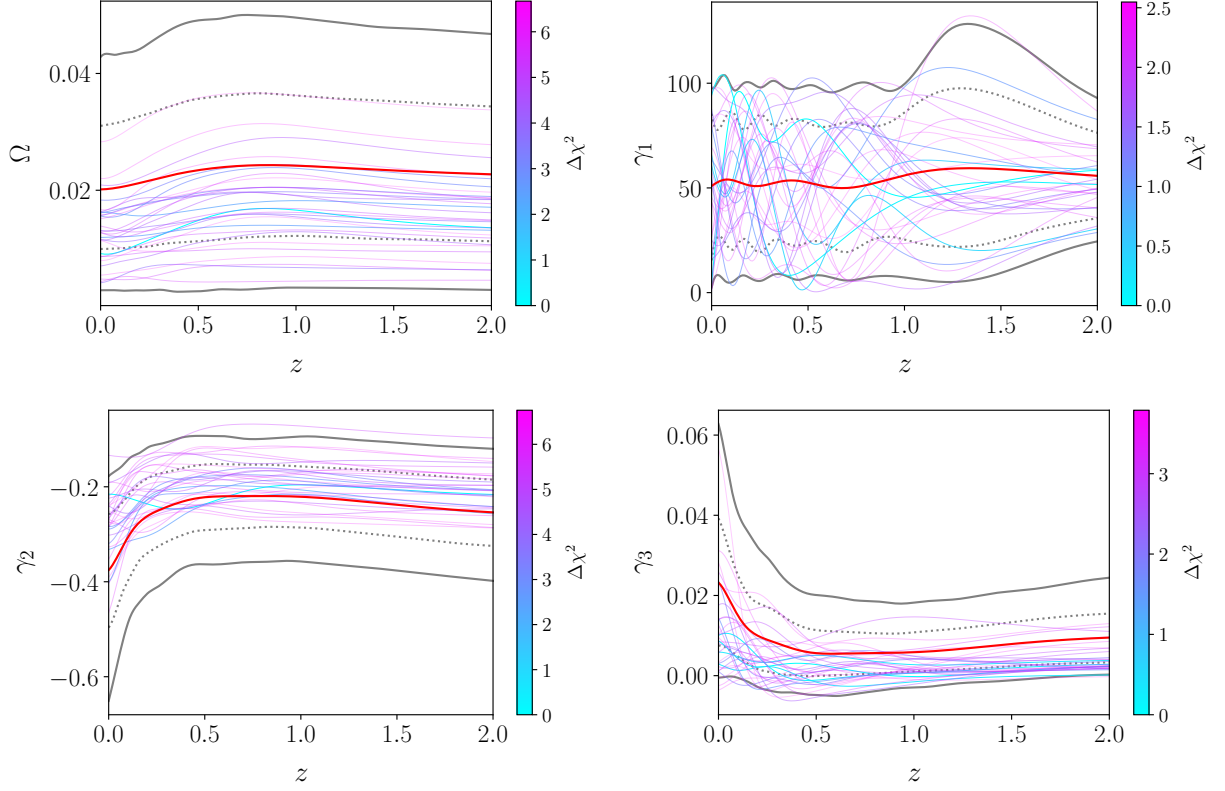


FIG. 6. Constraints on function shape of $\{\Omega, \gamma_1, \gamma_2, \gamma_3\}$ in the same style as Fig. 2.

Parameters	Λ CDM	w_0w_a CDM	Quintessence	Thawing Gravity
$100\omega_b$	$2.226(2.227) \pm 0.013$	$2.222(2.221) \pm 0.013$	$22.30(22.34) \pm 0.013$	$2.230(2.222) \pm 0.012$
$100\omega_c$	$11.857(11.830) \pm 0.081$	$11.924(11.913) \pm 0.091$	$11.809(11.862) \pm 0.012$	$11.810(11.759) \pm 0.077$
H_0 [km/s/Mpc]	$67.74(67.85) \pm 0.36$	$67.93(68.06) \pm 0.73$	$66.94(66.95)^{+0.58}_{-0.49}$	$66.81(66.89)^{+0.54}_{-0.41}$
n_s	$0.9662(0.9668) \pm 0.0036$	$0.9648(0.9648) \pm 0.0037$	$0.9677(0.9673) \pm 0.0037$	$0.9674(0.9672) \pm 0.0035$
$\ln 10^{10} A_s$	$3.042(3.044) \pm 0.014$	$3.035(3.030) \pm 0.014$	$3.046(3.045) \pm 0.014$	$3.044(3.058) \pm 0.013$
τ	$0.0558(0.573) \pm 0.0069$	$0.0519(0.0491) \pm 0.0071$	$0.0582(0.0506) \pm 0.0073$	$0.0571(0.0569) \pm 0.068$
w_0	N.A.	$-0.83(-0.83) \pm 0.06$	$-0.968(-0.970)^{+0.011}_{-0.030}$	$-0.92(-0.89)^{+0.03}_{-0.05}$
w_a	N.A.	$-0.71(-0.73)^{+0.29}_{-0.25}$	$0.006(-0.006)^{+0.033}_{-0.048}$	$-0.19(-0.27)^{+0.13}_{-0.12}$
ξ	N.A.	N.A.	N.A.	$< 0.74(0.61)$
λ	N.A.	N.A.	N.A.	$1.19(1.41)^{+0.42}_{-0.30}$
$V_0/3H_0^2$	N.A.	N.A.	N.A.	$0.723(0.723)^{+0.008}_{-0.021}$

TABLE II. Bestfit values (in parenthesis) and 1σ posterior constraints for the cosmological and model parameters of all models analyzed in the paper. In the case of one-sided posteriors, we report the 2σ range. Note that (w_0, w_a) are *not* parameters in the Thawing Gravity model; in this case, we report the effective (w_0, w_a) obtained by least-square fitting the CPL parameterization Eq.(9) to the full $w_{DE}(z)$ of *Thawing Gravity* in $0 < z < 1$.

	Λ CDM	w_0w_a CDM	Quintessence	Thawing Gravity
CMB	10972.6	10970	10972.9	10970.8
DESI BAO	15.8	12.4	18.6	13.7
SNIa	1404.8	1403.4	1402.8	1402.9
Total	12393.2	12385.8	12394.3	12387.4

TABLE III. Bestfit per experiment and total χ^2 of all models studied in this paper.

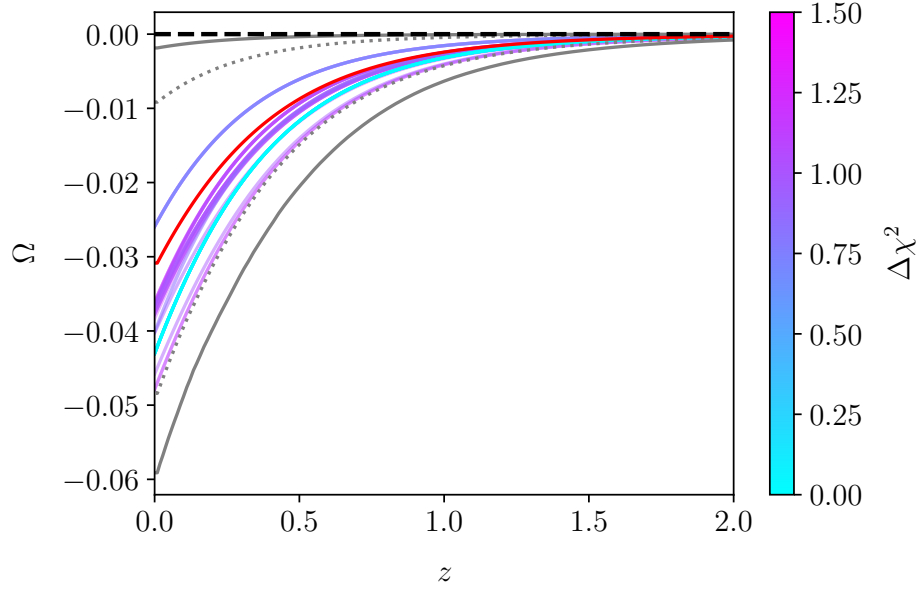


FIG. 7. Posterior of the corresponding EFT function Ω of the *Thawing Gravity* model derived from the MCMC chains, in the same plotting style as Fig. 2.

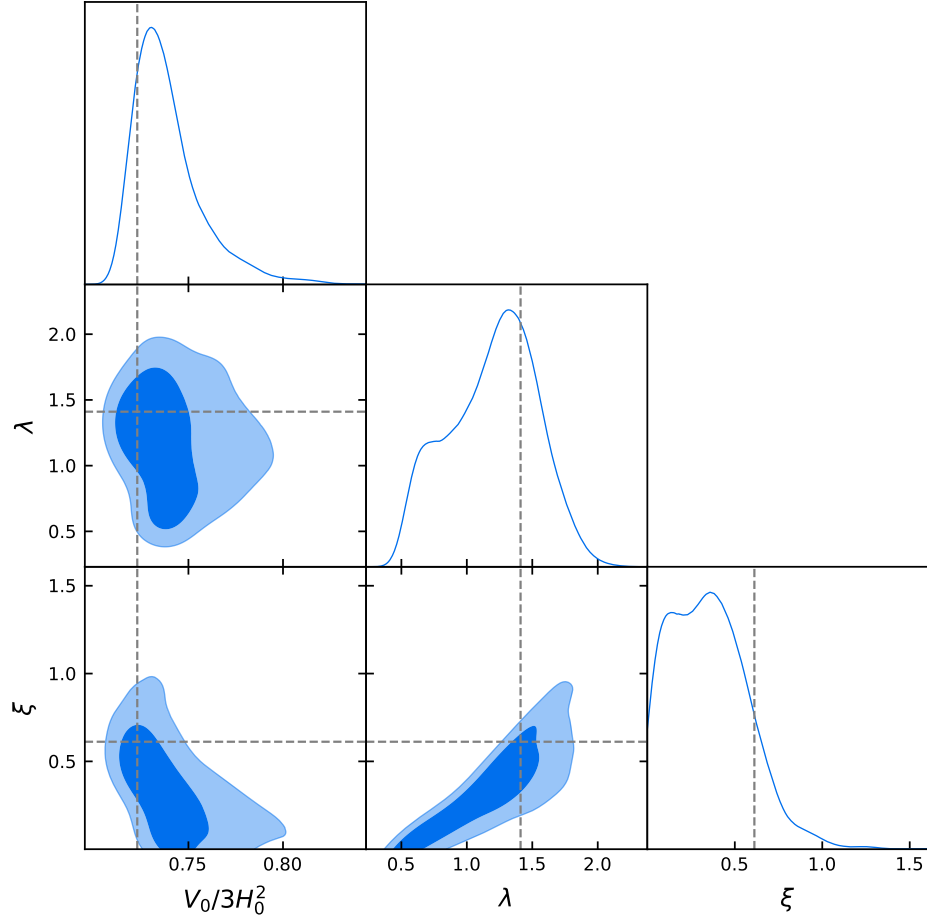


FIG. 8. Marginalized 68% and 95% posterior distributions of the model parameters of *Thawing Gravity*. Gray dashed lines mark the position of the bestfit point.

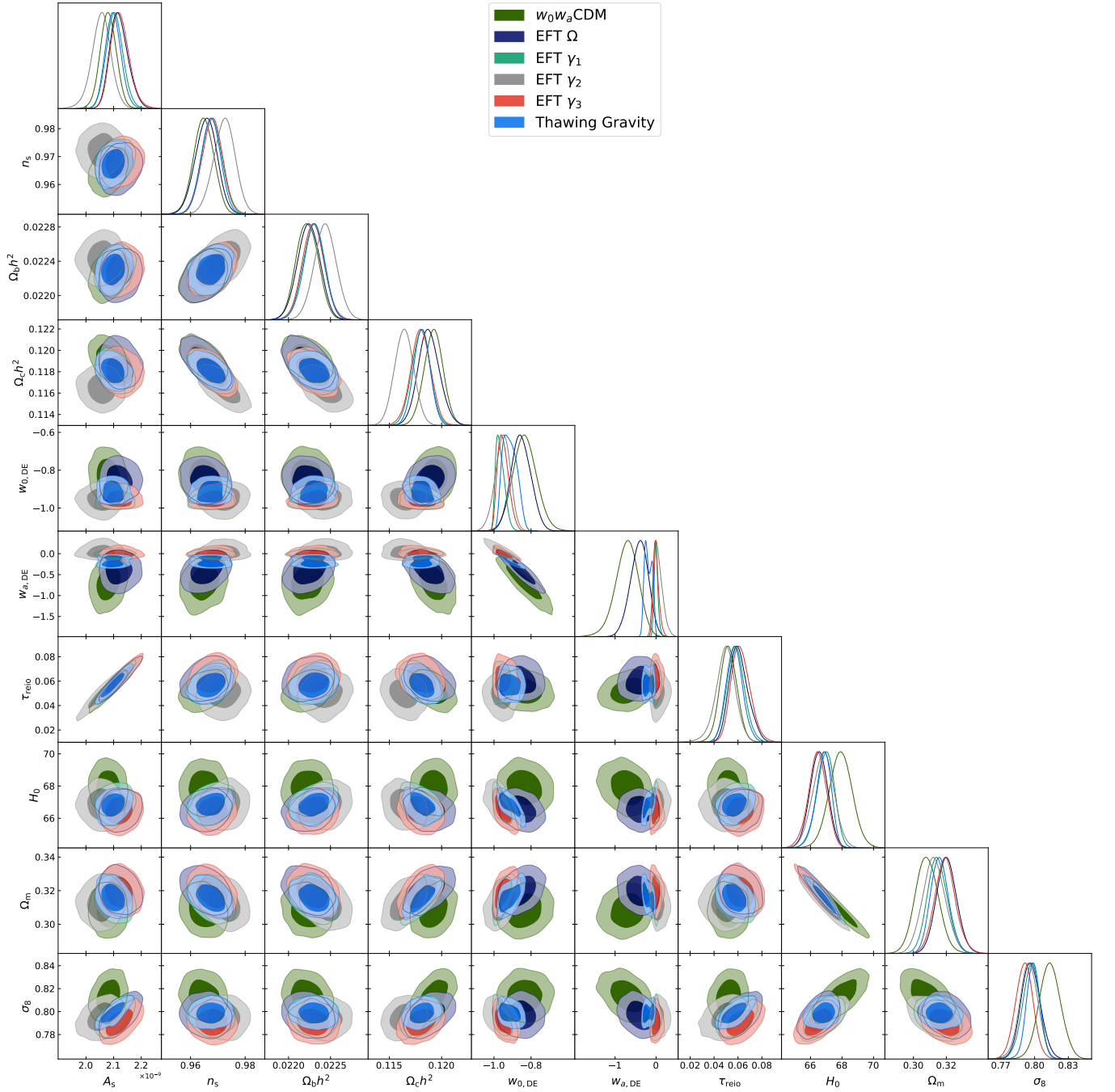


FIG. 9. 68% and 95% marginalized posterior distributions of cosmological parameters in all the models studied.

Fig. 8 plots the posterior distributions of the Lagrangian parameters $\{\xi, V_0, \lambda\}$ of *Thawing Gravity* (5), while the posterior distributions of all cosmological parameters are reported in Fig. 9. As mentioned in the main text, we use α (8) as one of the parameters to sample in the MCMC procedure. Still we present our results for the posteriors in terms of the Lagrangian parameter ξ . Also, the Lagrangian parameter V_0 is not really free, rather we fix it via a shooting algorithm, to reproduce H_0 today. Therefore in this Appendix we present our analysis specifications and results in terms of the dimensionless combination $V_0/3H_0^2$. Bestfit values and 1σ constraints of the parameters are reported in Table II. The total and per experiment bestfit χ^2 are presented in Table III.

-
- [1] A. G. Adame *et al.* (DESI), (2024), [arXiv:2404.03002 \[astro-ph.CO\]](#).
- [2] A. G. Adame *et al.* (DESI), (2024), [arXiv:2404.03000 \[astro-ph.CO\]](#).
- [3] M. Chevallier and D. Polarski, *Int. J. Mod. Phys. D* **10**, 213 (2001), [arXiv:gr-qc/0009008](#).
- [4] E. V. Linder, *Phys. Rev. Lett.* **90**, 091301 (2003), [arXiv:astro-ph/0208512](#).
- [5] D. Scolnic *et al.*, *Astrophys. J.* **938**, 113 (2022), [arXiv:2112.03863 \[astro-ph.CO\]](#).
- [6] D. Rubin *et al.*, (2023), [arXiv:2311.12098 \[astro-ph.CO\]](#).
- [7] T. M. C. Abbott *et al.* (DES), (2024), [arXiv:2401.02929 \[astro-ph.CO\]](#).
- [8] R. Calderon *et al.* (DESI), (2024), [arXiv:2405.04216 \[astro-ph.CO\]](#).
- [9] K. Lodha *et al.* (DESI), (2024), [arXiv:2405.13588 \[astro-ph.CO\]](#).
- [10] L. Orchard and V. H. Cárdenas, (2024), [arXiv:2407.05579 \[astro-ph.CO\]](#).
- [11] A. Chudaykin and M. Kunz, (2024), [arXiv:2407.02558 \[astro-ph.CO\]](#).
- [12] G. Alestas, M. Delgado, I. Ruiz, Y. Akrami, M. Montero, and S. Nesseris, (2024), [arXiv:2406.09212 \[hep-th\]](#).
- [13] H. Wang and Y.-S. Piao, (2024), [arXiv:2404.18579 \[astro-ph.CO\]](#).
- [14] A. Notari, M. Redi, and A. Tesi, (2024), [arXiv:2406.08459 \[astro-ph.CO\]](#).
- [15] I. D. Gialamas, G. Hütsi, K. Kannike, A. Racioppi, M. Raidal, M. Vasar, and H. Veermäe, (2024), [arXiv:2406.07533 \[astro-ph.CO\]](#).
- [16] O. Akarsu, A. De Felice, E. Di Valentino, S. Kumar, R. C. Nunes, E. Ozulker, J. A. Vazquez, and A. Yadav, (2024), [arXiv:2406.07526 \[astro-ph.CO\]](#).
- [17] J. J. Heckman, O. F. Ramadan, and J. Sakstein, (2024), [arXiv:2406.04408 \[astro-ph.CO\]](#).
- [18] O. F. Ramadan, J. Sakstein, and D. Rubin, (2024), [arXiv:2405.18747 \[astro-ph.CO\]](#).
- [19] P. Mukherjee and A. A. Sen, (2024), [arXiv:2405.19178 \[astro-ph.CO\]](#).
- [20] W. Giarè, M. A. Sabogal, R. C. Nunes, and E. Di Valentino, (2024), [arXiv:2404.15232 \[astro-ph.CO\]](#).
- [21] K. V. Berghaus, J. A. Kable, and V. Miranda, (2024), [arXiv:2404.14341 \[astro-ph.CO\]](#).
- [22] W. Yin, *JHEP* **05**, 327 (2024), [arXiv:2404.06444 \[hep-ph\]](#).
- [23] Y. Tada and T. Terada, *Phys. Rev. D* **109**, L121305 (2024), [arXiv:2404.05722 \[astro-ph.CO\]](#).
- [24] B. R. Dinda, (2024), [arXiv:2405.06618 \[astro-ph.CO\]](#).
- [25] M. Cortès and A. R. Liddle, (2024), [arXiv:2404.08056 \[astro-ph.CO\]](#).
- [26] V. Patel and L. Amendola, (2024), [arXiv:2407.06586 \[astro-ph.CO\]](#).
- [27] G. Liu, Y. Wang, and W. Zhao, (2024), [arXiv:2407.04385 \[astro-ph.CO\]](#).
- [28] G. Efstathiou (2024) [arXiv:2406.12106 \[astro-ph.CO\]](#).
- [29] D. Wang, (2024), [arXiv:2404.13833 \[astro-ph.CO\]](#).
- [30] Y. Carloni, O. Luongo, and M. Muccino, (2024), [arXiv:2404.12068 \[astro-ph.CO\]](#).
- [31] E. O. Colgáin, M. G. Dainotti, S. Capozziello, S. Pourojaghi, M. M. Sheikh-Jabbari, and D. Stojkovic, (2024), [arXiv:2404.08633 \[astro-ph.CO\]](#).
- [32] O. Luongo and M. Muccino, (2024), [arXiv:2404.07070 \[astro-ph.CO\]](#).
- [33] Z. Huang *et al.*, (2024), [arXiv:2405.03983 \[astro-ph.CO\]](#).
- [34] X. D. Jia, J. P. Hu, and F. Y. Wang, (2024), [arXiv:2406.02019 \[astro-ph.CO\]](#).
- [35] Z. Wang, S. Lin, Z. Ding, and B. Hu, (2024), [arXiv:2405.02168 \[astro-ph.CO\]](#).
- [36] D. Shlivko and P. J. Steinhardt, *Phys. Lett. B* **855**, 138826 (2024), [arXiv:2405.03933 \[astro-ph.CO\]](#).
- [37] P. Creminelli, G. D’Amico, J. Norena, and F. Vernizzi, *JCAP* **02**, 018 (2009), [arXiv:0811.0827 \[astro-ph\]](#).
- [38] B. Feng, X.-L. Wang, and X.-M. Zhang, *Phys. Lett. B* **607**, 35 (2005), [arXiv:astro-ph/0404224](#).
- [39] S. Peirone, M. Martinelli, M. Raveri, and A. Silvestri, *Phys. Rev. D* **96**, 063524 (2017), [arXiv:1702.06526 \[astro-ph.CO\]](#).
- [40] G. W. Horndeski, *Int. J. Theor. Phys.* **10**, 363 (1974).
- [41] B. Hu, M. Raveri, N. Frusciante, and A. Silvestri, *Phys. Rev. D* **89**, 103530 (2014), [arXiv:1312.5742 \[astro-ph.CO\]](#).
- [42] M. Raveri, B. Hu, N. Frusciante, and A. Silvestri, *Phys. Rev. D* **90**, 043513 (2014), [arXiv:1405.1022 \[astro-ph.CO\]](#).
- [43] A. Lewis, A. Challinor, and A. Lasenby, *Astrophys. J.* **538**, 473 (2000), [arXiv:astro-ph/9911177 \[astro-ph\]](#).
- [44] J. K. Bloomfield, E. E. Flanagan, M. Park, and S. Watson, *JCAP* **08**, 010 (2013), [arXiv:1211.7054 \[astro-ph.CO\]](#).
- [45] G. Gubitosi, F. Piazza, and F. Vernizzi, *JCAP* **02**, 032 (2013), [arXiv:1210.0201 \[hep-th\]](#).
- [46] N. Frusciante, G. Papadomanolakis, and A. Silvestri, *JCAP* **07**, 018 (2016), [arXiv:1601.04064 \[gr-qc\]](#).
- [47] A. De Felice, N. Frusciante, and G. Papadomanolakis, *JCAP* **03**, 027 (2017), [arXiv:1609.03599 \[gr-qc\]](#).
- [48] F. Gerardi, M. Martinelli, and A. Silvestri, *JCAP* **07**, 042 (2019), [arXiv:1902.09423 \[astro-ph.CO\]](#).
- [49] N. Frusciante, G. Papadomanolakis, S. Peirone, and A. Silvestri, *JCAP* **02**, 029 (2019), [arXiv:1810.03461 \[gr-qc\]](#).
- [50] M. Raveri, P. Bull, A. Silvestri, and L. Pogosian, *Phys. Rev. D* **96**, 083509 (2017), [arXiv:1703.05297 \[astro-ph.CO\]](#).
- [51] S. Peirone, K. Koyama, L. Pogosian, M. Raveri, and A. Silvestri, *Phys. Rev. D* **97**, 043519 (2018), [arXiv:1712.00444 \[astro-ph.CO\]](#).
- [52] J. Espejo, S. Peirone, M. Raveri, K. Koyama, L. Pogosian, and A. Silvestri, *Phys. Rev. D* **99**, 023512 (2019), [arXiv:1809.01121 \[astro-ph.CO\]](#).
- [53] A. Adams, N. Arkani-Hamed, S. Dubovsky, A. Nicolis, and R. Rattazzi, *JHEP* **10**, 014 (2006), [arXiv:hep-th/0602178](#).
- [54] D. de Boe, G. Ye, F. Renzi, I. S. Albuquerque, N. Frusciante, and A. Silvestri, (2024), [arXiv:2403.13096 \[astro-ph.CO\]](#).
- [55] B. Hu, M. Raveri, N. Frusciante, and A. Silvestri, (2014), [arXiv:1405.3590 \[astro-ph.IM\]](#).
- [56] C. Deffayet, O. Pujolas, I. Sawicki, and A. Vikman, *JCAP* **10**, 026 (2010), [arXiv:1008.0048 \[hep-th\]](#).

- [57] E. Bellini and I. Sawicki, *JCAP* **07**, 050 (2014), [arXiv:1404.3713 \[astro-ph.CO\]](#).
- [58] E. Rosenberg, S. Gratton, and G. Efstathiou, *Mon. Not. Roy. Astron. Soc.* **517**, 4620 (2022), [arXiv:2205.10869 \[astro-ph.CO\]](#).
- [59] N. Aghanim *et al.* (Planck), *Astron. Astrophys.* **641**, A5 (2020), [arXiv:1907.12875 \[astro-ph.CO\]](#).
- [60] J. Carron, M. Mirmelstein, and A. Lewis, *JCAP* **09**, 039 (2022), [arXiv:2206.07773 \[astro-ph.CO\]](#).
- [61] J. Torrado and A. Lewis, *JCAP* **05**, 057 (2021), [arXiv:2005.05290 \[astro-ph.IM\]](#).
- [62] J. Torrado and A. Lewis, “Cobaya: Bayesian analysis in cosmology,” *Astrophysics Source Code Library*, record ascl:1910.019 (2019).
- [63] A. Gelman and D. B. Rubin, *Statist. Sci.* **7**, 457 (1992).
- [64] J. J. Bennett, G. Buldgen, P. F. De Salas, M. Drewes, S. Gariazzo, S. Pastor, and Y. Y. Y. Wong, *JCAP* **04**, 073 (2021), [arXiv:2012.02726 \[hep-ph\]](#).
- [65] J. Froustey, C. Pitrou, and M. C. Volpe, *JCAP* **12**, 015 (2020), [arXiv:2008.01074 \[hep-ph\]](#).
- [66] K. Akita and M. Yamaguchi, *JCAP* **08**, 012 (2020), [arXiv:2005.07047 \[hep-ph\]](#).
- [67] Y. Yang, X. Ren, Q. Wang, Z. Lu, D. Zhang, Y.-F. Cai, and E. N. Saridakis, (2024), [arXiv:2404.19437 \[astro-ph.CO\]](#).
- [68] M. Raveri, L. Pogosian, M. Martinelli, K. Koyama, A. Silvestri, and G.-B. Zhao, *JCAP* **02**, 061 (2023), [arXiv:2107.12990 \[astro-ph.CO\]](#).
- [69] L. Pogosian, M. Raveri, K. Koyama, M. Martinelli, A. Silvestri, G.-B. Zhao, J. Li, S. Peirone, and A. Zucca, *Nature Astron.* **6**, 1484 (2022), [arXiv:2107.12992 \[astro-ph.CO\]](#).
- [70] N. Frusciante, S. Peirone, S. Casas, and N. A. Lima, *Phys. Rev. D* **99**, 063538 (2019), [arXiv:1810.10521 \[astro-ph.CO\]](#).
- [71] M. Raveri, *Phys. Rev. D* **101**, 083524 (2020), [arXiv:1902.01366 \[astro-ph.CO\]](#).
- [72] A. J. Ross, L. Samushia, C. Howlett, W. J. Percival, A. Burden, and M. Manera, *Mon. Not. Roy. Astron. Soc.* **449**, 835 (2015), [arXiv:1409.3242 \[astro-ph.CO\]](#).
- [73] S. Alam *et al.* (BOSS), *Mon. Not. Roy. Astron. Soc.* **470**, 2617 (2017), [arXiv:1607.03155 \[astro-ph.CO\]](#).
- [74] S. Alam *et al.* (eBOSS), *Phys. Rev. D* **103**, 083533 (2021), [arXiv:2007.08991 \[astro-ph.CO\]](#).
- [75] M. Asgari *et al.* (KiDS), *Astron. Astrophys.* **645**, A104 (2021), [arXiv:2007.15633 \[astro-ph.CO\]](#).
- [76] A. Amon *et al.* (DES), *Phys. Rev. D* **105**, 023514 (2022), [arXiv:2105.13543 \[astro-ph.CO\]](#).
- [77] L. F. Secco *et al.* (DES), *Phys. Rev. D* **105**, 023515 (2022), [arXiv:2105.13544 \[astro-ph.CO\]](#).
- [78] T. M. C. Abbott *et al.* (Kilo-Degree Survey, Dark Energy Survey), *Open J. Astrophys.* **6**, 2305.17173 (2023), [arXiv:2305.17173 \[astro-ph.CO\]](#).
- [79] V. Poulin, T. L. Smith, T. Karwal, and M. Kamionkowski, *Phys. Rev. Lett.* **122**, 221301 (2019), [arXiv:1811.04083 \[astro-ph.CO\]](#).
- [80] P. Agrawal, F.-Y. Cyr-Racine, D. Pinner, and L. Randall, *Phys. Dark Univ.* **42**, 101347 (2023), [arXiv:1904.01016 \[astro-ph.CO\]](#).
- [81] M.-X. Lin, G. Benevento, W. Hu, and M. Raveri, *Phys. Rev. D* **100**, 063542 (2019), [arXiv:1905.12618 \[astro-ph.CO\]](#).
- [82] F. Niedermann and M. S. Sloth, *Phys. Rev. D* **103**, L041303 (2021), [arXiv:1910.10739 \[astro-ph.CO\]](#).
- [83] G. Ye and Y.-S. Piao, *Phys. Rev. D* **101**, 083507 (2020), [arXiv:2001.02451 \[astro-ph.CO\]](#).
- [84] M. Braglia, M. Ballardini, F. Finelli, and K. Koyama, *Phys. Rev. D* **103**, 043528 (2021), [arXiv:2011.12934 \[astro-ph.CO\]](#).
- [85] G. Ye and A. Silvestri, (2024), [arXiv:2407.02471 \[astro-ph.CO\]](#).
- [86] H. Wang, Z.-Y. Peng, and Y.-S. Piao, (2024), [arXiv:2406.03395 \[astro-ph.CO\]](#).
- [87] L. Pogosian, G.-B. Zhao, and K. Jedamzik, (2024), [arXiv:2405.20306 \[astro-ph.CO\]](#).
- [88] Y. Toda, W. Giarè, E. Özülker, E. Di Valentino, and S. Vagnozzi, (2024), [arXiv:2407.01173 \[astro-ph.CO\]](#).
- [89] G. P. Lynch, L. Knox, and J. Chluba, (2024), [arXiv:2406.10202 \[astro-ph.CO\]](#).
- [90] O. Seto and Y. Toda, (2024), [arXiv:2405.11869 \[astro-ph.CO\]](#).
- [91] F. J. Qu, K. M. Surrao, B. Bolliet, J. C. Hill, B. D. Sherwin, and H. T. Jense, (2024), [arXiv:2404.16805 \[astro-ph.CO\]](#).
- [92] I. J. Allali, A. Notari, and F. Rompineve, (2024), [arXiv:2404.15220 \[astro-ph.CO\]](#).
- [93] A. Lewis, (2019), [arXiv:1910.13970 \[astro-ph.IM\]](#).